Hemoglobin phase of oxygenation and deoxygenation in early brain development measured using fNIRS

Hama Watanabe[a,1], Yoshihiko Shitara[b], Yoshinori Aoki[b], Takanobu Inoue[b], Shinya Tsuchida[b], Naoto Takahashi[b], and Gentaro Taga[a]

[a]Graduate School of Education, The University of Tokyo, Tokyo 113-0033, Japan; and [b]Department of Pediatrics, Graduate School of Medicine, The University of Tokyo, Tokyo 113-0033, Japan

Edited by Marcus E. Raichle, Washington University in St. Louis, St. Louis, MO, and approved January 18, 2017 (received for review October 14, 2016)

A crucial issue in neonatal medicine is the impact of preterm birth on the developmental trajectory of the brain. Although a growing number of studies have shown alterations in the structure and function of the brain in preterm-born infants, we propose a method to detect subtle differences in neurovascular and metabolic functions in neonates and infants. Functional near-infrared spectroscopy (fNIRS) was used to obtain time-averaged phase differences between spontaneous low-frequency (less than 0.1 Hz) oscillatory changes in oxygenated hemoglobin (oxy-Hb) and those in deoxygenated hemoglobin (deoxy-Hb). This phase difference was referred to as hemoglobin phase of oxygenation and deoxygenation (hPod) in the cerebral tissue of sleeping neonates and infants. We examined hPod in term, late preterm, and early preterm infants with no evidence of clinical issues and found that all groups of infants showed developmental changes in the values of hPod from an in-phase to an antiphase pattern. Comparison of hPod among the groups revealed that developmental changes in hPod in early preterm infants precede those in late preterm and term infants at term equivalent age but then, progress at a slower pace. This study suggests that hPod measured using fNIRS is sensitive to the developmental stage of the integration of circular, neurovascular, and metabolic functions in the brains of neonates and infants.

fNIRS | infant | preterm | Hb | neurovascular

Birth is a drastic event for the developing brain, because this is when the oxygen supply switches from the fetal–placental circulation to an autonomous system. In addition, the extrauterine environment begins to provide the neonate with a tremendous flow of stimuli. Earlier exposure to the extrauterine environment is thought to influence the developmental trajectory of the brain. It has long been known that preterm birth affects brain development and is associated with a higher rate of neurodevelopmental impairment (1). A growing number of MRI studies have shown that preterm-born neonates and infants have brain structures with aberrant volumes, morphologies, and networks at term equivalent (2, 3) and school age (4, 5). Studies of resting-state fMRI have also shown that the functional connectivity of the cortex is different in term and preterm infants (6). However, it is a matter of controversy whether neonatal MRI of the brain can predict long-term adverse outcomes, such as minor neurological dysfunction (7, 8). Given the fact that preterm birth before 37 wk of gestation accounts for more than 10% of all live births (9), we need a practical and safe method to detect the status of brain development in newborns.

The development of the brain involves underlying hemodynamic and metabolic changes (10). Near-infrared spectroscopy (NIRS) has been used to measure cerebral blood concentrations of oxygenated Hb (oxy-Hb) and deoxygenated Hb (deoxy-Hb) at the bedside and estimate cerebral blood volume, oxygen saturation (SO_2), cerebral blood flow (CBF), and cerebral metabolic rate of oxygen ($CMRO_2$) in neonates (11, 12). Previous studies in premature infants indicate that SO_2 decreases with chronological age (CA), regardless of gestational age (GA), and that $CMRO_2$ increases with postmenstrual age (PMA). These findings suggest that circulatory development occurs with increasing CA and that neural development proceeds with increasing PMA (13, 14). Although quantitative assessments of CBF and metabolism have been intensively studied in typically and atypically developing neonates and infants (15), the development of the dynamic properties of hemodynamics and metabolism remains to be uncovered.

In the mature brain, neural activity induces both regional CBF and oxygen metabolism (16). The typical hemodynamic response to neural activation consists of an increase in oxy-Hb and an almost antiphase decrease in deoxy-Hb. As a method of neuroimaging, functional NIRS (fNIRS) has been used to reveal the hemodynamic response to stimulus-induced cortical activation in young infants (17–21) and preterm infants (22). fNIRS has also been used to study the functional connectivity of the cortex using temporal correlations of spontaneous low-frequency oscillations (less than 0.1 Hz) of the Hb signals in multiple regions of the cortex in infants (23–25). Although both oxy- and deoxy-Hb signal changes represent hemodynamic responses to neural activity, the relative phase between the oxy- and deoxy-Hb signals reflects complex interplay among neurovascular and metabolic processes (16, 26, 27). Studies of the spontaneous fluctuations of oxy- and deoxy-Hb in the cortex of sleeping infants have shown the presence of stable phase differences between oxy- and deoxy-Hb signals (25, 28). However, limited information is available regarding age-dependent changes in Hb phase differences in typically and atypically developing brains.

According to a model used to relate the tissue concentration and saturation of Hb to hemodynamic and metabolic processes (26), in-phase oscillations of oxy- and deoxy-Hb are associated with changes in total Hb concentration in the blood and partial blood volume, whereas antiphase oscillations are associated with changes in SO_2 in the blood, the $CMRO_2$, and the speed of CBF. The superposition of these signals predicts only in-phase or antiphase patterns of oxy- and deoxy-Hb changes. To predict

Significance

We propose time-averaged hemoglobin phase of oxygenation and deoxygenation (hPod) measured using functional near-infrared spectroscopy as a method for the detection of the developmental status of the hemodynamic and metabolic processes of the brain. hPod values exhibit initially rapid changes from in-phase to antiphase patterns in neonates and infants. These changes become more gradual in later development. We also describe the impact of early preterm birth on brain development.

Author contributions: H.W., N.T., and G.T. designed research; H.W., Y.S., Y.A., T.I., S.T., N.T., and G.T. performed research; H.W. and G.T. contributed new reagents/analytic tools; H.W. and G.T. analyzed data; and H.W. and G.T. wrote the paper.

The authors declare no conflict of interest.

This article is a PNAS Direct Submission.

[1]To whom correspondence should be addressed. Email: hama@p.u-tokyo.ac.jp.

This article contains supporting information online at www.pnas.org/lookup/suppl/doi:10.1073/pnas.1616866114/-/DCSupplemental.

intermediate phase patterns, signals originating from different types of vasculature, such as arterioles, capillaries, and venules, have been superimposed (26, 29, 30). Theoretical considerations of hemodynamic and metabolic processes in different types of vasculature suggest that phase differences between oxy- and deoxy-Hb changes provide important information regarding the structure and function of the neurovascular system.

In this study, we refer to the time-averaged phase differences between spontaneous oscillatory changes in oxy-Hb and those of deoxy-Hb as hemoglobin phase of oxygenation and deoxygenation (hPod). It is assumed that hPod is sensitive to the complex interplay between neurovascular and metabolic changes and developmental status. We hypothesize that hPod may be used to detect subtle differences in development between term- and preterm-born infants without explicit clinical issues. We also show theoretical considerations for understanding the mechanism of changes in hPod.

Results

An NIRS instrument (ETG-100; Hitachi Medical Corporation) with 10 measurement channels (five channels in each hemisphere) was used in this study to detect relative concentration changes in oxy- and deoxy-Hb (millimolar·millimeter) with a 0.1-s time resolution, from which hPod was calculated (*SI Materials and Methods*). When the neonate or infant was in natural sleep in a dimly lit room, he or she was held by a nurse or measurement staff. The measurements began after the NIRS probe was placed around the infant's head. Data obtained from 100 infants, including neonates admitted to the neonatal intensive care unit (NICU) of the University of Tokyo Hospital, were used for the final analysis of the study (*Materials and Methods*, *Data Analysis*). The infants were categorized into three groups according to their GAs at birth: (*i*) 24 term infants (GA $\geq$ 37 wk, range: 37–41 wk), (*ii*) 32 late preterm infants (34 wk $\leq$ GA $\leq$ 36 wk), and (*iii*) 44 early preterm infants (GA < 34 wk, range: 23–33 wk). To examine typical development around 2–4 mo of age, data from 59 full-term healthy infants were also analyzed in the study. The characteristics of the infants are shown in Table S1.

Measurement and analysis times for each group are shown in Table S2. The measurements lasted ~7 min in a room at the NICU for infants in the hospital. They lasted 10 min in an outpatient care room for infants who were out of the hospital and the control infants ages 2–4 mo. We detected periods containing motion artifacts in the oxy- and deoxy-Hb time series data and excluded them from hPod analysis.

Fig. 1 shows individual hPod values in each measurement. The value of hPod in individual measurement was calculated as the vector average of hPod values among the 10 measurement channels. Fig. 1*A* presents the hPod values as a function of PMA, and Fig. 1*B* presents the same values as a function of CA. Zero and 2π indicate an in-phase pattern between oxy- and deoxy-Hb changes, and π indicates an antiphase pattern of changes. Thus, a value larger than $3/2\pi$ indicates a pattern close to an in-phase one, whereas a value smaller than $3/2\pi$ indicates a pattern close to an antiphase one. Each group's dataset (combined term plus control, which is referred to as "term," late preterm, and early preterm) was fitted using a logarithmic trend line. We calculated developmental curves for hPod as a function of PMA (Fig. 1*A*) ($R^2 = 0.70861$, 0.58153, and 0.13753 for term, late preterm, and early preterm infants, respectively). In the same way, we also obtained developmental curves for hPod as a function of CA (Fig. 1*B*) ($R^2 = 0.66871$, 0.69471, and 0.24867 for term, late preterm, and early preterm infants, respectively).

Each of the hPod developmental curves indicated a decrease from a pattern close to an in-phase one to one close to an antiphase pattern. As shown in Fig. 1*A*, the developmental curves in the term and late preterm groups (Fig. 1*A*, blue and green lines, respectively) have an initial rapid decrease and a subsequent slow decrease in response to increasing PMA. The values of hPod in the early preterm group (Fig. 1*A*, red line) are relatively low before a PMA of 40 wk. This result suggests that, because neonates/infants in the early preterm group have lived longer in the extrauterine environment at the time of the measurements, the developmental change in the hPod value may be a preceding event. However, the hPod value in the early preterm group is eventually overtaken by those of the other two infant groups later in development. The same dataset rearranged as a function of CA reveals that all three groups have similar initial decreases in the value of hPod as shown in Fig. 1*B*. Remarkably, this finding suggests that an initial rapid decrease in the hPod value depends on CA rather than PMA. After the neonatal period, the hPod values in the term and late preterm groups continue to decrease gradually with increasing CA, whereas the rate of the decrease is slow in the early preterm group.

Longitudinal measurements were performed in 4 term, 9 late preterm, and 10 early preterm infants starting from the neonatal period up to 6 mo of CA (Fig. 2). The measurements were completed two to four times for each infant (Table S1). These longitudinal data indicate the presence of developmental patterns similar to those obtained using the cross-sectional measurement in Fig. 1.

To investigate developmental properties immediately after birth, we focused on the data obtained during the neonatal period, which were measured between 34 wk, 0 d and 43 wk, 6 d (PMA). Individual measurement data for infants in each GA group (i.e., term, late preterm, or early preterm) were categorized into the three following measurement periods based on PMA at the time of measurement: (*i*) 34–36 wk (from 34 wk, 0 d to 36 wk, 6 d), (*ii*) 37–39 wk (from 37 wk, 0 d to 39 wk, 6 d), and (*iii*) 40–43 wk (from 40 wk, 0 d to 43 wk, 6 d). When measurements from an infant were obtained multiple times during this neonatal period, the first valid set of data at the earliest measurement time was included in the following group comparison. Fig. 3 shows vector representations of the value of hPod for each group of infants during each measurement period. The black and colored arrows in Fig. 3 indicate individual and mean hPod values, respectively. Group means and variances of hPod values (rad) are also shown in Table S3.

To investigate group differences in the vector values of hPod during each measurement period, we performed a Watson–Williams test (31), and to determine which group combinations were significantly different from the others, the Tukey–Welsch procedure was used (*SI Materials and Methods*, *Data Analysis*, *Statistical analysis*). At 37–39 wk (PMA), statistical analyses revealed a significant difference in mean hPod values among three infant groups ($F[2, 44] = 4.454$, $P = 0.05$). A multiple comparison showed that the mean hPod value in the early preterm group was smaller than that of the term group ($P = 0.05$). A significant group difference was also observed at 40–43 wk (PMA) ($F[2, 27] = 11.513$, $P = 0.001$). The mean hPod values in the late preterm group and the early preterm group were smaller than that of the term group ($P = 0.01$ and $P = 0.001$, respectively). These results indicate that preterm infants have more antiphase hPod values compared with term infants at the same PMA. At 34–36 wk (PMA), the hPod value in the early preterm group was smaller than that of the late preterm group. However, this difference was not significant ($P = 0.123$). The data obtained immediately after birth indicate that a rapid change in the hPod value from an in-phase to an antiphase pattern depends on the CA rather than the PMA.

We analyzed all of the data, including those obtained during the neonatal period and in early infancy. Individual data points in each of the GA groups (i.e., term, late preterm, and early preterm) were categorized into the three following CA periods at the time of the measurement: (*i*) 0–7 wk (from 0 wk, 1 d to 7 wk, 6 d),

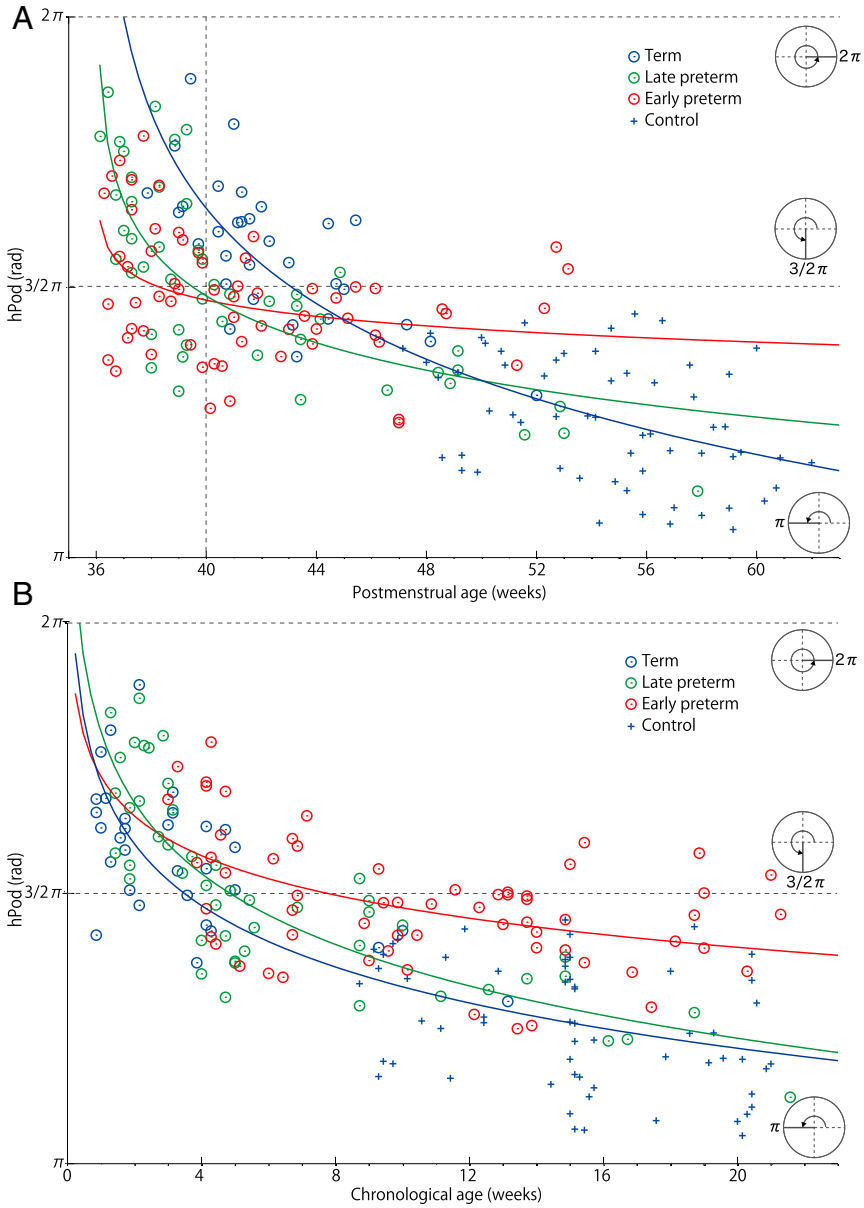

Fig. 1. Development of hPod in different groups of infants classified by GA. (*A*) Individual values of hPod (rad) viewed as a function of PMA (weeks). (*B*) Individual values of hPod (rad) viewed as a function of CA (weeks). hPod values of 2π and π correspond to in-phase and antiphase changes in the oxy- and deoxy-Hb signals, respectively. Blue, green, and red circles indicate the data for term, late preterm, and early preterm infants, respectively, and + indicates the data for control infants. Logarithmic trend lines fitted to data from the combined term plus control, late preterm, and early preterm infants are shown using blue, green, and red lines, respectively.

(*ii*) 8–13 wk (from 8 wk, 0 d to 13 wk, 6 d), and (*iii*) 14–21 wk (from 14 wk, 0 d to 21 wk, 6 d). Fig. 4 shows a vector representation of the hPod value for each group of infants during each CA measurement period. The black and colored arrows in Fig. 4 indicate individual and mean hPod values, respectively. Group means and variances of hPod values (rad) are also shown in Table S4.

Statistical analyses of the data obtained during 8–13 wk (CA) revealed a significant difference in the mean hPod values of three infant groups ($F[2, 49] = 9.661$, $P = 0.001$). A multiple comparison showed that the mean hPod value in the term group was smaller than that of the early preterm group ($P = 0.001$). At 14–21 wk (CA), the group difference was significant ($F[2, 61] = 24.164$, $P = 0.001$), and mean hPod values in the term group and the late preterm group were significantly smaller than that of the early preterm group ($P = 0.001$ and $P = 0.01$, respectively). At 0–7 wk (CA), no significant differences among the term, late preterm, and early preterm groups were observed. These results indicate that three different GA groups of infants exhibit similar hPod values with patterns close to in phase until 2 mo of CA. In contrast, developmental changes of hPod values toward an antiphase pattern in early preterm infants are slower than those of the term and late preterm infants at 3–6 mo of CA.

As a reference value for the hPod, we performed analysis of adults using the previously published data by Sasai et al. (32). The mean value of hPod obtained from 20 adults is shown in Fig. S1.

We used a model by Fantini (26) and Hill's equation for Hb SO_2 to derive a mathematical model for changes in the concentrations of oxy- and deoxy-Hb in tissues with multiple vessels

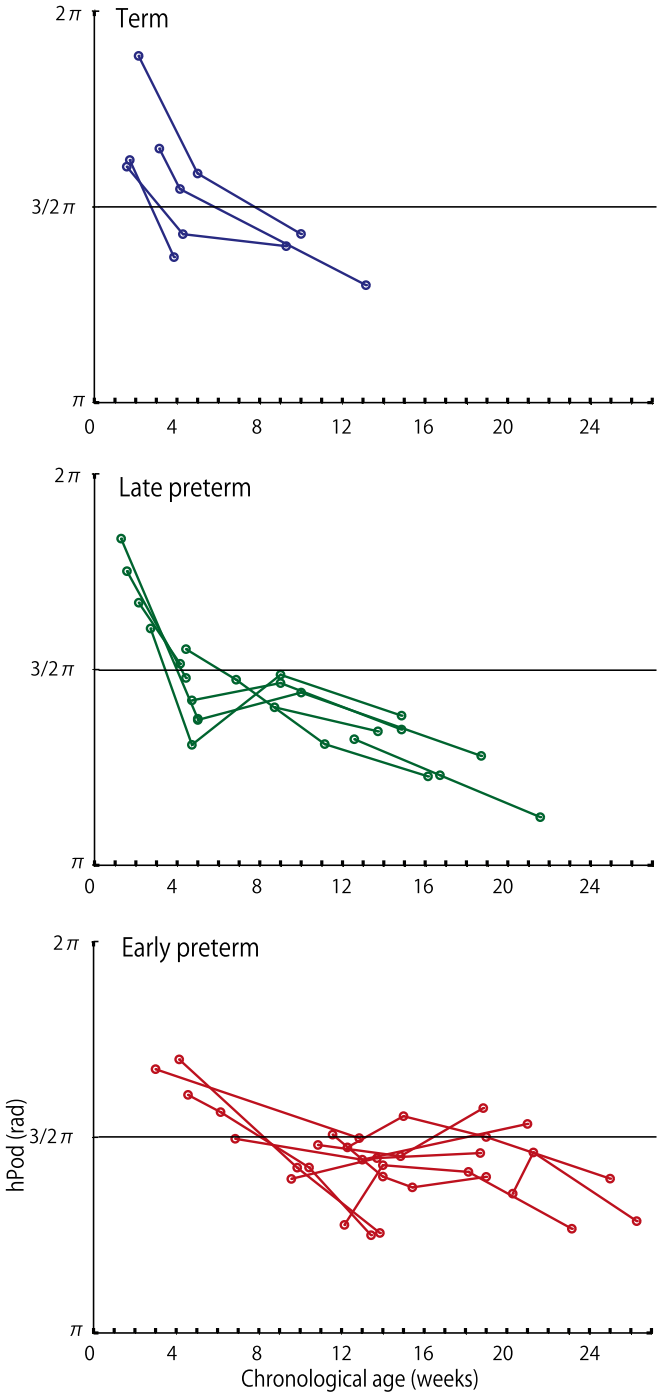

Fig. 2. Longitudinal development of hPod values (rad) from individual infants as a function of CA (weeks). The hPod values (rad) that were repeatedly measured within the same infant are connected with lines. *Top*, *Middle*, and *Bottom* show the data from term, late preterm, and early preterm infants, respectively.

$[\Delta[oxy\text{-}Hb]^{(\text{tissue})\text{MV}}$ and $\Delta[deoxy\text{-}Hb]^{(\text{tissue})\text{MV}}]$ expressed by summation of normalized changes in partial pressure of oxygen $\Delta PO_2{}^{(i)}$ $(i = a, c, v)$, partial blood volume $\Delta V_{bv}^{(i)}$ $(i = a, c, v)$, oxygen utilization rate $\Delta\alpha_{\dot{O}_2}$, and speed of blood flow $\Delta c^{(c)}$, where the superscripts a, c, and v indicate the arterial, capillary, and venous Hb compartments, respectively. We show a possible mechanism for the developmental changes in hPod based on the analysis of the mathematical model as shown in Fig. 5.

Discussion

This study shows that the values of hPod generally decrease from an in-phase to an antiphase pattern as a function of age, regardless of the group as classified by GA. This decrease consists of a rapid change occurring at birth and a gradual change lasting during the first 6 mo of CA. The rapid decrease of hPod with increasing CA until 8 wk of age was observed in both term and late preterm infants. The early preterm infants had lower values of hPod in the neonatal periods until 44 wk PMA, suggesting that the early preterm infants had an advanced development. The early preterm infants, however, also had a slower decrease in the hPod value after 8 wk CA. These findings show that hPod is sensitive to subtle differences in blood flow and metabolism, reflecting differential brain development in term/late preterm and early preterm infants with no apparent clinical issues.

In-Phase Pattern of hPod During Neonatal Periods. As shown in Fig. 5, higher values of hPod (i.e., in phase) in early CA periods may be accounted for by a dominance of the in-phase contributions of ΔV_{bv} over the antiphase contributions of ΔPO_2, which is obtained under the condition with lower baseline values of PO_2 (Eqs. **6** and **7**). The model also assumes that oxygen extraction occurs only in capillaries, so that antiphase contributions of $\Delta\alpha_{\dot{O}_2}$ and Δc are present only in these vessels. However, because capillaries are not yet well-developed at earlier CAs (33), it is likely that the antiphase contributions of $\Delta\alpha_{\dot{O}_2}$ and Δc are limited during the neonatal period.

Rapid Change of hPod from an In-Phase to an Antiphase Pattern with Increasing CA. The rapid initial decrease in the value of hPod with increasing CA, which is observed in all of the GA groups of infants, may be induced by physiological switches occurring at birth (i.e., "debut" into extrauterine environment). The model suggests that a rapid increase in the antiphase contribution of ΔPO_2 compared with the in-phase contributions of ΔV_{bv} may account for this phenomenon (Eqs. **6** and **7** and Fig. 5). Although how the fluctuation of ΔPO_2 is generated is not clear, it is likely that the

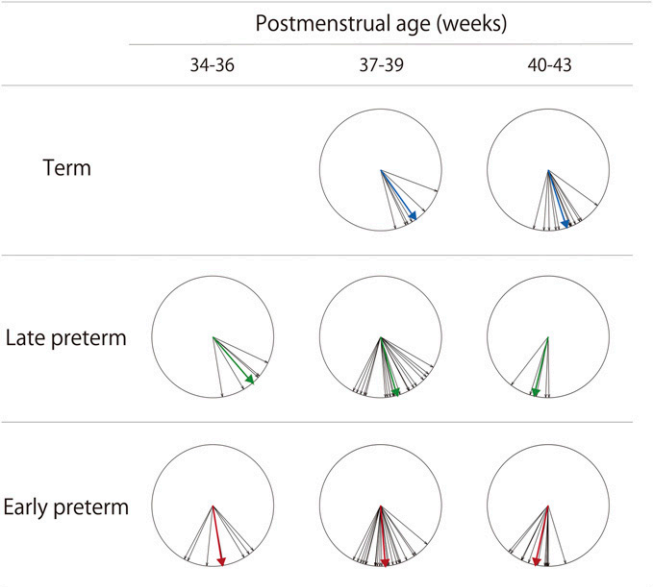

Fig. 3. Developmental changes in hPod values during the neonatal period. Vector representations of individual and averaged hPod values (black and colored arrows, respectively) during three measurement periods (34–36, 37–39, and 40–43 wk PMA) are shown for each infant group (term, late preterm, and early preterm).

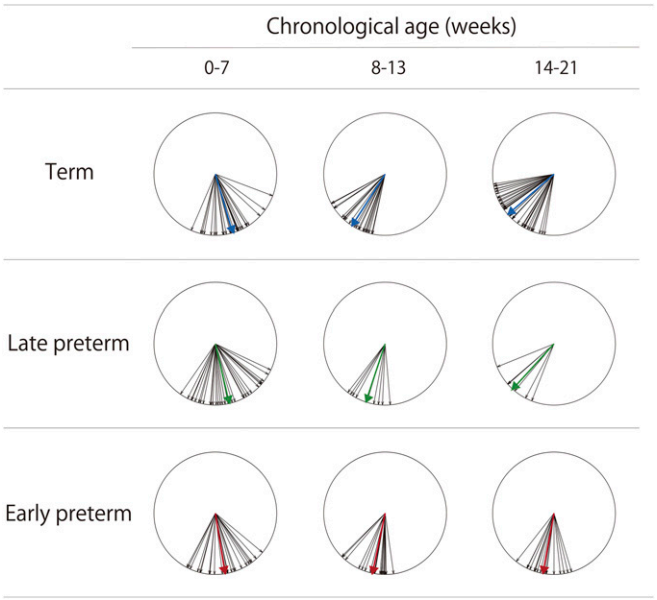

Fig. 4. Developmental changes in hPod values during the first one-half of the first year after birth. Vector representations of individual and averaged values (black and colored arrows, respectively) during three measurement periods (0–7, 8–13, and 14–21 wk CA) are shown for each infant group (term plus control referred to as term, late preterm, and early preterm).

fluctuation reflects the regulation by the circular system, including the lung and heart, which are rapidly developing. In particular, the shift of oxygen dissociation curve (34) to the right induces increase of the antiphase contribution of ΔPO_2. Thus, it is likely that the rapid adaptation of the circulatory system to the extrauterine environment may affect the changes in hPod. The CA-dependent changes in hPod are consistent with the facts that the transition from fetal to adult Hb starts at birth, regardless of GA, and that hematocrit decreases faster in more premature infants (35). Note that the hPod value is not affected by the decrease in [tot-Hb] or hematocrit but is affected by the increase in the oxygen affinity of Hb from the fetal to adult type. Previous assessments of CBF and oxygen metabolism in premature infants using fNIRS also showed that only cerebral tissue SO_2 undergoes a decrease as a function of CA until around 6–8 wk, and it was speculated that this observation might be cause by a decrease in hematocrit (12–14). According to the aforementioned model, a decrease in cerebral tissue SO_2 is not induced by the decrease in concentration of Hb or hematocrit but is induced by the change in the oxygen affinity of Hb.

As one of the important features of cerebral circulatory control, cerebral autoregulation provides a constant CBF over a wide range of cerebral perfusion pressures. Because autoregulation is not yet fully developed in neonates (36–38), it is important to consider whether the development of autoregulation affects changes in hPod. According to the dynamic model of tissue concentration and SO_2, which is an extended version of the model used in this study (29), autoregulation contributes to in-phase patterns of oxy- and deoxy-Hb changes. Because these changes are in the opposite direction from those observed during development, the development of autoregulation is most likely not a major factor in the development of hPod. The antiphase contributions of $\Delta\alpha_{O2}$ and Δc may also be present, but these effects may be limited because of the gradual development of capillaries (33).

Gradual Changes in hPod Toward an Antiphase Pattern After 8-wk CA. After the periods of rapid decrease in hPod values, gradual decreases in the value of hPod were observed in all of the GA groups of infants. These decreases led to the observation of more antiphase hPod values. According to the model (Eqs. **6** and **7** and Fig. 5), the recruitment of capillaries leads to higher antiphase contribution of $\Delta\alpha_{\dot{O}_2}$ and Δc to hPod. Previous studies have shown that a transient increase in oxygen consumption induced by neural activation is outpaced by increases in blood flow caused by the dilation of arteriole vessels in the mature brain (39–41). Thus, the mature form of neurovascular coupling is represented as an antiphase pattern consisting of increases in oxy-Hb and decreases in deoxy-Hb caused by blood flow increases in adults (16) and infants as young as 3 mo of age (17). As shown by the model, the effects of $\Delta\alpha_{\dot{O}_2}$ and Δc on oxy- and deoxy-Hb concentration changes are in opposite directions. Mature neurovascular coupling leads to Δc playing a more dominant role than $\Delta\alpha_{\dot{O}_2}$ as a contributor to the hPod value. Although blood oxygenation level-dependent (BOLD) (42–46) and oxy- and deoxy-Hb (47, 48) responses are controversial during the early development of neurovascular coupling, we speculate that the gradual changes in the value of hPod toward an antiphase pattern may reflect the increasing antiphase contribution of Δc in capillaries with angiogenesis that actively occurs in the first one-half of the first year of life after birth.

We further speculate that changes in capillary blood flow induced by neural activity may be facilitated by the synaptogenesis that may occur in concert with angiogenesis. It is well-known that the synaptic architecture of humans rapidly develops during the first one-half of the first year of life and has been thought to form the basis for functional development of the brain under the vast stream of sensory input from the environment (49). However, an anatomical study indicated that capillary formation starts between term and 3 mo postnatal (33). Thus, the development of vascular networks has been thought to proceed in parallel with neural development (50). Animal studies have also provided evidence to support the interdependence between angiogenesis and synaptogenesis (51–53). In a previous study in premature infants, baseline CBF values and the metabolic rate of oxygen increased with PMA but did not increase with CA, suggesting that these changes are based on the gradual development of the neurovascular system (14).

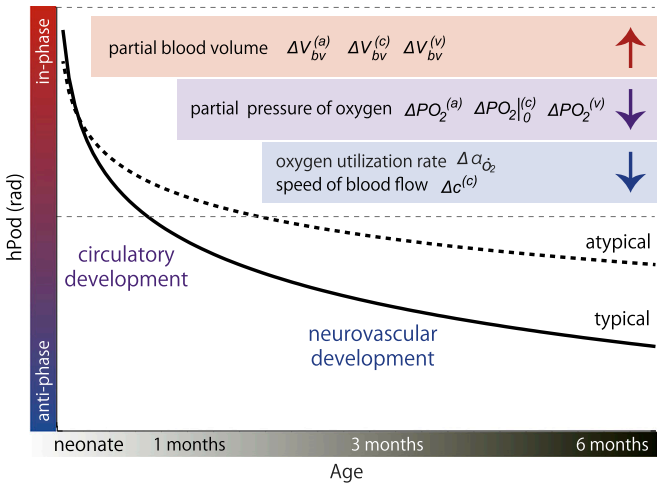

Fig. 5. Possible contributions of hemodynamic and metabolic variables to development of hPod. ΔV_{bv}, ΔPO_2, $\Delta\alpha_{\dot{O}_2}$, and Δc indicate changes in partial blood volume, partial pressure of oxygen, oxygen utilization rate, and speed of blood flow, respectively. Upward and downward arrows mean contributions to in-phase and antiphase patterns, respectively. Solid and dotted lines are identical to the fitted curves of term plus control and early preterm infants, respectively, in Fig. 1*B*.

Impact of Early Preterm Birth on Brain Development. One of the important findings of this study is that measurements of hPod revealed the impact of early preterm birth on brain development, even in infants with no apparent explicit clinical issues at the time of our measurements. We showed that early preterm infants had a different pattern of hPod development compared with late preterm and term infants. The value of hPod was lower than that of term infants in early preterm infants at the same PMAs (37–39 and 40–43 wk), suggesting that early preterm infants may have an advanced development of their circulatory processes after birth. However, early preterm infants had a slower development of the value of hPod compared with late preterm and term infants at later CAs (after 8–13 wk). This finding suggests that the structural and/or functional aspects of the development of the neurovascular system may be altered during the first one-half of the first year of life in early preterm infants, although it is unknown whether these infants catch up to late preterm and term infants later in life.

As a different methodology for assessing the development of metabolism in the brain, magnetic resonance spectroscopy has been used to determine the developmental profiles of metabolites, such as a marker of axonal and neuronal development, an energy metabolite, and a membrane metabolite, and indicated that the period between birth and 3 mo of age is an immensely active period in metabolite development (54). A comparison of metabolic maturation in preterm-born infants with that of term infants further showed that the metabolic maturation in preterm-born infants, at term equivalence, preceded development in term infants but then, progressed at a slower pace and trajectory (55). This developmental profile found in preterm infants, which is quite similar to the one that we observe with hPod using fNIRS, suggests that preterm birth influences both the early onset of and long-term alterations in the function of the neurovascular system.

hPod as a Clinical Tool. Previous studies using fMRI and fNIRS have relied on a single parameter of BOLD, oxy-Hb or deoxy-Hb, to infer neural activation. However, hPod measured using fNIRS contains integrated information regarding the interplays among the neural activity, blood flow, and metabolism. The stability of hPod is based solely on the timing of changes in the oxy- and deoxy-Hb signals and the relative concentration changes obtained using standard fNIRS devices using diffuse NIR light, which is sufficient to calculate the value of hPod. Measurement of the absolute concentrations of Hb signals, which require frequency- and time-domain devices (12, 56, 57), is not required to obtain the value of hPod. The measurement of hPod is also based on spontaneous changes in Hb signals in a period less than 10 min and does not require the repetition of stimuli or an assumption regarding the hemodynamic response. Thus, hPod provides information regarding the dynamic properties of neurovascular function in addition to baseline values of physiological parameters accumulated through a large number of previous studies on CBF and metabolism in typically and atypically developing infants (15, 56). hPod measured using fNIRS is a practical bedside tool, which can be used to assess the developmental status of the neurovascular system of the brain.

Materials and Methods

Participants. We examined 184 infants who were admitted to the NICU of the University of Tokyo Hospital. Neonates or infants scheduled to be discharged from the hospital within 3 d were eligible for the first measurement of the study. One hundred infants were included for the analysis (Table S1). They were categorized into the following three groups based on GA at birth: (*i*) 24 term infants (GA ≥ 37 wk, range: 37–41 wk), (*ii*) 32 late preterm infants (34 wk ≤ GA ≤ 36 wk), and (*iii*) 44 early preterm infants (GA < 34 wk, range: 23–33 wk); 4 term, 9 late preterm, and 10 early preterm infants were measured multiple times (Table S1).

To examine the typical development of hPod at around 2–4 mo of postterm age, 59 full-term healthy infants (29 girls and 30 boys; mean birth weight: 3,132.2 g, range: 2,476–4,270 g; mean GA: 39.1 wk, range: 37–42 wk) were enrolled in the study (Table S1). PMAs at the time of measurement were between 47 and 62 wk. Ethical approval for this study was granted by the Office for Life Science Research Ethics and Safety of The University of Tokyo, and the Research Ethics Committee of the Graduate School of Medicine and Faculty of Medicine of The University of Tokyo. Written informed consent was obtained from the parent(s) of all infants before the initiation of the measurements.

Procedure. We began the measurements when the neonates or infants were in natural sleep. Nurses or measurement staff held the neonates or infants, and the fNIRS probes were placed around their heads. We turned off the room lights and made the room as quiet as possible. The measurements were conducted in a room of the NICU when neonates or infants were in the hospital and an outpatient care room after the infants were out of the hospital. The measurements of control infants ages 2–4 mo were conducted in the infant laboratory. Details are in *SI Materials and Methods*.

Data Analysis. We detected periods containing motion artifacts in the oxy- and deoxy-Hb time series data and excluded them from hPod analysis. The method of exclusion is detailed in *SI Materials and Methods*. Then, oxy- and deoxy-Hb time course signals were filtered through a frequency band of 0.05–0.1 Hz using a fast Fourier transform (FFT) to remove physiological noise (e.g., heartbeats and respirations) and measurement noise (e.g., slow signal drifts and high-frequency noise). The effect of band-pass filtering on hPod is also described in *SI Results* (Figs. S2 and S3).

Calculation of hPod. To obtain instantaneous phases of the signal, a Hilbert transformation was applied as follows:

$$\tilde{s}(t)=\frac{1}{\pi}\int_{-\infty}^{\infty}\frac{s(\tau)}{t-\tau}d\tau s(t), \quad [1]$$

where $\tilde{s}(t)$ is a Hilbert transform of $s(t)$.

Instantaneous phase $\theta(t)$ is then calculated as

$$\theta(t)=arctan\left(\frac{\tilde{s}(t)}{s(t)}\right). \quad [2]$$

The phase difference between the instantaneous phases of oxy- and deoxy-Hb signals was calculated as follows:

$$\phi(t)=\theta_{oxy}(t)-\theta_{deoxy}(t). \quad [3]$$

Then, the hPod was determined using the following equation:

$$re^{ihPod}=\frac{1}{T}\int_{0}^{T}e^{i\phi(t)}dt, \quad [4]$$

where r is the strength of the phase difference. and *hPod* is the time average phase difference between oxy- and deoxy-Hb changes.

Finally, the channel-averaged values of hPod were obtained.

A Model of the Concentration and SO_2 of Hb in Tissue. Fantini (26) proposed a model to relate tissue concentration and saturation of Hb to hemodynamic and metabolic processes involving the serial compartments of arterioles, capillaries, and venules. It is assumed that oxygen extraction occurs only in the capillaries. The equations of the model are shown in *SI Materials and Methods*. To examine the effect of the postnatal changes in oxygenation affinity of the blood, we further used Hill's equation (34) for Hb SO_2 as a function of partial pressure of oxygen PO_2 as follows:

$$SO_2^{(i)}=\frac{PO_2^{(i)n}}{PO_2^{(i)n}+K^n}, \quad (i=a,c,v), \quad [5]$$

where n and K are parameters to be fitted to the curve of SO_2 (n = 2.5 and K = 25 for adults and n = 2.5 and K = 20 for newborns as shown in Fig. S4), and the superscripts *a*, *c*, and *v* indicate the arterial, capillary, and venous Hb compartments, respectively. Based on this model, we derived changes in the concentrations of oxy- and deoxy-Hb in tissues with multiple vessels [$\Delta[oxy\text{-}Hb]^{(tissue)MV}$ and $\Delta[deoxy\text{-}Hb]^{(tissue)MV}$] within the probed volume V and interpreted the physiological parameters that may affect the observed changes in the values of hPod as follows:

$$\Delta[oxy\text{-}Hb]^{(tissue)MV} = p^{(a)}\left(r_1^{(a)}\frac{\Delta PO_2{}^{(a)}}{PO_2{}^{(a)}} + \frac{\Delta V_{bv}^{(a)}}{V_{bv}^{(a)}}\right) + p^{(c)}\left[q_1{}^{(c)}\left(r_1^{(c)}\frac{\Delta PO_2|_0^{(c)}}{PO_2|_0^{(c)}} + \frac{\Delta V_{bv}^{(c)}}{V_{bv}^{(c)}}\right) + q_2{}^{(c)}\left(-\frac{\Delta\alpha_{\dot{O}_2}}{\alpha_{\dot{O}_2}} + \frac{\Delta c^{(c)}}{c^{(c)}}\right)\right] + p^{(v)}\left(r_1^{(v)}\frac{\Delta PO_2{}^{(v)}}{PO_2{}^{(v)}} + \frac{\Delta V_{bv}^{(v)}}{V_{bv}^{(v)}}\right) \quad [6]$$

and

$$\Delta[deoxy\text{-}Hb]^{(tissue)MV} = p^{(a)}\left(-r_1^{(a)}\frac{\Delta PO_2{}^{(a)}}{PO_2{}^{(a)}} + r_2{}^{(a)}\frac{\Delta V_{bv}^{(a)}}{V_{bv}^{(a)}}\right) + p^{(c)}\left[-q_1{}^{(c)}r_1^{(c)}\frac{\Delta PO_2|_0^{(c)}}{PO_2|_0^{(c)}} + r_2{}^{(c)}\left(q_1{}^{(c)}\right)\frac{\Delta V_{bv}^{(c)}}{V_{bv}^{(c)}} - q_2{}^{(c)}\left(-\frac{\Delta\alpha_{\dot{O}_2}}{\alpha_{\dot{O}_2}} + \frac{\Delta c^{(c)}}{c^{(c)}}\right)\right] + p^{(v)}\left(-r_1^{(v)}\frac{\Delta PO_2{}^{(v)}}{PO_2{}^{(v)}} + r_2{}^{(v)}\frac{\Delta V_{bv}^{(v)}}{V_{bv}^{(v)}}\right), \quad [7]$$

where $PO_2{}^{(i)}$, $V_{bv}^{(i)}$, $\alpha_{\dot{O}_2}$, and $c^{(c)}$ are variables describing partial pressure of oxygen, partial blood volume, oxygen utilization rate, and the speed of blood flow, respectively. $\Delta[oxy\text{-}Hb]^{(tissue)MV}$ and $\Delta[deoxy\text{-}Hb]^{(tissue)MV}$ are expressed by summation of normalized changes $\Delta PO_2{}^{(i)}$ ($i = a, c,$ and v), $\Delta V_{bv}^{(i)}$ ($i = a, c,$ and v), $\Delta\alpha_{\dot{O}_2}$, and $\Delta c^{(c)}$ with coefficients $p^{(i)}$, $q_1^{(c)}$, $q_2^{(c)}$, $r_1{}^{(i)}$, and $r_2{}^{(i)}$ ($i = a, c,$ and v). All of the coefficients are positive functions of physiological parameters as follows:

$$p^{(i)} = SO_2^{(i)}\left(PO_2^{(i)}\right)[tot\text{-}Hb]^{(blood)}\frac{V_{bv}^{(i)}}{V}, \quad (i = a, c, v), \quad [8]$$

where $[tot\text{-}Hb]$ is total Hb concentration;

$$q_1^{(c)} = \left(1 - e^{-\frac{\alpha_{\dot{O}_2}L_{bv}^{(c)}}{c^{(c)}}}\right)\frac{c^{(c)}}{\alpha_{\dot{O}_2}L_{bv}^{(c)}} \quad [9]$$

and

$$q_2^{(c)} = \left\{1 - e^{-\frac{\alpha_{\dot{O}_2}L_{bv}^{(c)}}{c^{(c)}}}\left(\frac{\alpha_{\dot{O}_2}L_{bv}^{(c)}}{c^{(c)}} + 1\right)\right\}\frac{c^{(c)}}{\alpha_{\dot{O}_2}L_{bv}^{(c)}}, \quad [10]$$

where $L_{bv}^{(c)}$ is a length of the capillary; and

$$r_1^{(i)} = \frac{PO_2^{(i)}}{SO_2^{(i)}}\frac{\partial SO_2^{(i)}}{\partial PO_2^{(i)}} = \frac{nK^n}{PO_2^{(i)n} + K^n}, \quad (i = a, c, v), \quad [11]$$

$$r_2^{(i)} = \frac{1 - SO_2^{(i)}}{SO_2^{(i)}} = \frac{K^n}{PO_2^{(i)n}}, \quad (i = a, v), \quad [12]$$

and

$$r_2^{(c)} = \frac{1 - SO_2|_0^{(c)}q_1^{(c)}}{SO_2|_0^{(c)}} = \frac{K^n + \left(1 - q_1^{(c)}\right)PO_2^{(c)n}}{PO_2^{(c)n}}. \quad [13]$$

Eqs. **6** and **7** reveal that contributions of ΔV_{bv} to $\Delta[oxy\text{-}Hb]^{(tissue)MV}$ and $\Delta[deoxy\text{-}Hb]^{(tissue)MV}$ have the same signs (i.e., in-phase pattern), whereas contributions of ΔPO_2, $\Delta\alpha_{\dot{O}_2}$, and Δc to $\Delta[oxy\text{-}Hb]^{(tissue)MV}$ and $\Delta[deoxy\text{-}Hb]^{(tissue)MV}$ have opposite signs (i.e., antiphase pattern). We have further estimated relative contributions of these variables' changes to the signs of tissue Hb changes by scrutinizing the coefficients. Values of $q_1^{(c)}$ and $q_2^{(c)}$ were calculated as functions of $\alpha_{\dot{O}_2}L_{bv}^{(c)}/c^{(c)}$. If $L_{bv}^{(c)}$ approaches zero, $q_1^{(c)}$ and $q_2^{(c)}$ approach one and zero, respectively (Fig. S5). This calculation indicates that, when the volume of the capillary is small (i.e., the length of capillary is short), the contributions of terms, including $\Delta\alpha_{\dot{O}_2}$ and Δc, are small and that the terms, including ΔPO_2 and ΔV_{bv}, dominantly contribute to the tissue Hb changes. Then, the hPod value is mainly determined by a balance between in-phase contributions of ΔV_{bv} and antiphase contributions of ΔPO_2. If $L_{bv}{}^{(c)}$ is increased, $q_1{}^{(c)}$ and $q_2{}^{(c)}$ approach the same value (Fig. S5). This calculation indicates that the larger volume of the capillary leads to the larger contribution of the term including $\Delta\alpha_{\dot{O}_2}$ and Δc to antiphase pattern of hPod. Values of $r_1{}^{(i)}$ and $r_2{}^{(i)}$ determine relative contributions of $\Delta PO2$ and ΔVbv. Although the lower baseline value of PO_2 (less than 30 mmHg) produces the larger value of $r_2{}^{(i)}$, contributing to in-phase hPod value, the higher baseline value of PO_2 produces the larger value of $r_1{}^{(i)}$, contributing to antiphase hPod value (Fig. S6*A*). Furthermore, the shift of SO_2 curve of Hb from fetal to adult pattern, which is expressed by changes in values of K, leads to more contribution of $r_1{}^{(i)}$ to antiphase hPod value (Fig. S6 *B*–*D*).

ACKNOWLEDGMENTS. We thank Drs. Akira Oka and Riki Nishimura for support with data collection, Fumitaka Homae for discussions regarding brain development, and Shuntaro Sasai for discussions for processing of adult data. We also thank the members of the Developmental Brain Science Laboratory, Graduate School of Education, The University of Tokyo; Makiko Imai, Kayo Asakawa, Yoshiko Koda, Hirotaka Gima, Moe Kato, Yoshio Kobayashi, Shotaro Ishikawa, Tomoko Yoneyama, and Nobue Kanaya for assistance with data acquisition and Keiko Hirano for administrative assistance. This work was partly supported by Japan Society for Promotion of Science Grants-in-Aid for Scientific Research 26350924 (to H.W.) and 26220004 (to G.T.).

1. Volpe JJ (2009) Brain injury in premature infants: A complex amalgam of destructive and developmental disturbances. *Lancet Neurol* 8(1):110–124.
2. Inder TE, Warfield SK, Wang H, Hüppi PS, Volpe JJ (2005) Abnormal cerebral structure is present at term in premature infants. *Pediatrics* 115(2):286–294.
3. Ball G, et al. (2012) The effect of preterm birth on thalamic and cortical development. *Cereb Cortex* 22(5):1016–1024.
4. Zhang Y, et al. (2015) Cortical structural abnormalities in very preterm children at 7 years of age. *Neuroimage* 109:469–479.
5. Fischi-Gómez E, et al. (2015) Structural brain connectivity in school-age preterm infants provides evidence for impaired networks relevant for higher order cognitive skills and social cognition. *Cereb Cortex* 25(9):2793–2805.
6. Smyser CD, et al. (2016) Resting-state network complexity and magnitude are reduced in prematurely born infants. *Cereb Cortex* 26(1):322–333.
7. Nongena P, Ederies A, Azzopardi DV, Edwards AD (2010) Confidence in the prediction of neurodevelopmental outcome by cranial ultrasound and MRI in preterm infants. *Arch Dis Child Fetal Neonatal Ed* 95(6):F388–F390.
8. Setänen S, Lehtonen L, Parkkola R, Aho K, Haataja L; PIPARI Study Group (2016) Prediction of neuromotor outcome in infants born preterm at 11 years of age using volumetric neonatal magnetic resonance imaging and neurological examinations. *Dev Med Child Neurol* 58(7):721–727.
9. Blencowe H, et al.; Born Too Soon Preterm Birth Action Group (2013) Born too soon: The global epidemiology of 15 million preterm births. *Reprod Health* 10(Suppl 1):S2.
10. Raichle ME (2010) Two views of brain function. *Trends Cogn Sci* 14(4):180–190.
11. Ijichi S, et al. (2005) Developmental changes of optical properties in neonates determined by near-infrared time-resolved spectroscopy. *Pediatr Res* 58(3):568–573.
12. Franceschini MA, et al. (2007) Assessment of infant brain development with frequency-domain near-infrared spectroscopy. *Pediatr Res* 61(5 Pt 1):546–551.
13. Roche-Labarbe N, et al. (2010) Noninvasive optical measures of CBV, StO(2), CBF index, and rCMRO(2) in human premature neonates' brains in the first six weeks of life. *Hum Brain Mapp* 31(3):341–352.
14. Roche-Labarbe N, et al. (2012) Near-infrared spectroscopy assessment of cerebral oxygen metabolism in the developing premature brain. *J Cereb Blood Flow Metab* 32(3):481–488.
15. Brew N, Walker D, Wong FY (2014) Cerebral vascular regulation and brain injury in preterm infants. *Am J Physiol Regul Integr Comp Physiol* 306(11):R773–R786.
16. Obrig H, Villringer A (2003) Beyond the visible–imaging the human brain with light. *J Cereb Blood Flow Metab* 23(1):1–18.
17. Taga G, Asakawa K, Maki A, Konishi Y, Koizumi H (2003) Brain imaging in awake infants by near-infrared optical topography. *Proc Natl Acad Sci USA* 100(19):10722–10727.
18. Peña M, et al. (2003) Sounds and silence: An optical topography study of language recognition at birth. *Proc Natl Acad Sci USA* 100(20):11702–11705.
19. Homae F, Watanabe H, Nakano T, Asakawa K, Taga G (2006) The right hemisphere of sleeping infant perceives sentential prosody. *Neurosci Res* 54(4):276–280.
20. Watanabe H, Homae F, Nakano T, Taga G (2008) Functional activation in diverse regions of the developing brain of human infants. *Neuroimage* 43(2):346–357.
21. Sato H, et al. (2012) Cerebral hemodynamics in newborn infants exposed to speech sounds: A whole-head optical topography study. *Hum Brain Mapp* 33(9):2092–2103.
22. Mahmoudzadeh M, et al. (2013) Syllabic discrimination in premature human infants prior to complete formation of cortical layers. *Proc Natl Acad Sci USA* 110(12):4846–4851.
23. Homae F, et al. (2010) Development of global cortical networks in early infancy. *J Neurosci* 30(14):4877–4882.
24. White BR, Liao SM, Ferradal SL, Inder TE, Culver JP (2012) Bedside optical imaging of occipital resting-state functional connectivity in neonates. *Neuroimage* 59(3):2529–2538.
25. Imai M, et al. (2014) Functional connectivity of the cortex of term and preterm infants and infants with Down's syndrome. *Neuroimage* 85(Pt 1):272–278.
26. Fantini S (2002) A haemodynamic model for the physiological interpretation of in vivo measurements of the concentration and oxygen saturation of haemoglobin. *Phys Med Biol* 47(18):N249–N257.
27. Boas DA, Jones SR, Devor A, Huppert TJ, Dale AM (2008) A vascular anatomical network model of the spatio-temporal response to brain activation. *Neuroimage* 40(3):1116–1129.

28. Taga G, et al. (2000) Spontaneous oscillation of oxy- and deoxy- hemoglobin changes with a phase difference throughout the occipital cortex of newborn infants observed using non-invasive optical topography. *Neurosci Lett* 282(1-2):101–104.
29. Fantini S (2014) Dynamic model for the tissue concentration and oxygen saturation of hemoglobin in relation to blood volume, flow velocity, and oxygen consumption: Implications for functional neuroimaging and coherent hemodynamics spectroscopy (CHS). *Neuroimage* 85(Pt 1):202–221.
30. Sassaroli A, Kainerstorfer JM, Fantini S (2016) Nonlinear extension of a hemodynamic linear model for coherent hemodynamics spectroscopy. *J Theor Biol* 389:132–145.
31. Watson GS, Williams EJ (1956) On the construction of significance tests on the circle and the sphere. *Biometrika* 43(3/4):344–352.
32. Sasai S, Homae F, Watanabe H, Taga G (2011) Frequency-specific functional connectivity in the brain during resting state revealed by NIRS. *Neuroimage* 56(1):252–257.
33. Norman MG, O'Kusky JR (1986) The growth and development of microvasculature in human cerebral cortex. *J Neuropathol Exp Neurol* 45(3):222–232.
34. Hill AV (1910) The possible effects of the aggregation of the molecules of haemoglobin on its dissociation curves. *J Physiol* 40:4–7.
35. Dallman PR (1981) Anemia of prematurity. *Annu Rev Med* 32(1):143–160.
36. Lou HC, Lassen NA, Friis-Hansen B (1979) Impaired autoregulation of cerebral blood flow in the distressed newborn infant. *J Pediatr* 94(1):118–121.
37. Greisen G (2005) Autoregulation of cerebral blood flow in newborn babies. *Early Hum Dev* 81(5):423–428.
38. Gilmore MM, et al. (2011) Relationship between cerebrovascular dysautoregulation and arterial blood pressure in the premature infant. *J Perinatol* 31(11):722–729.
39. Kim SG, Ogawa S (2012) Biophysical and physiological origins of blood oxygenation level-dependent fMRI signals. *J Cereb Blood Flow Metab* 32(7):1188–1206.
40. Hillman EM (2014) Coupling mechanism and significance of the BOLD signal: A status report. *Annu Rev Neurosci* 37:161–181.
41. Gagnon L, et al. (2015) Quantifying the microvascular origin of BOLD-fMRI from first principles with two-photon microscopy and an oxygen-sensitive nanoprobe. *J Neurosci* 35(8):3663–3675.
42. Yamada H, et al. (1997) A rapid brain metabolic change in infants detected by fMRI. *Neuroreport* 8(17):3775–3778.
43. Born P, et al. (1998) Visual activation in infants and young children studied by functional magnetic resonance imaging. *Pediatr Res* 44(4):578–583.
44. Arichi T, et al. (2010) Somatosensory cortical activation identified by functional MRI in preterm and term infants. *Neuroimage* 49(3):2063–2071.
45. Harris JJ, Reynell C, Attwell D (2011) The physiology of developmental changes in BOLD functional imaging signals. *Dev Cogn Neurosci* 1(3):199–216.
46. Kozberg MG, Chen BR, DeLeo SE, Bouchard MB, Hillman EM (2013) Resolving the transition from negative to positive blood oxygen level-dependent responses in the developing brain. *Proc Natl Acad Sci USA* 110(11):4380–4385.
47. Watanabe H, Homae F, Taga G (2012) Activation and deactivation in response to visual stimulation in the occipital cortex of 6-month-old human infants. *Dev Psychobiol* 54(1):1–15.
48. Roche-Labarbe N, et al. (2014) Somatosensory evoked changes in cerebral oxygen consumption measured non-invasively in premature neonates. *Neuroimage* 85(Pt 1): 279–286.
49. Huttenlocher PR (1990) Morphometric study of human cerebral cortex development. *Neuropsychologia* 28(6):517–527.
50. Andreone BJ, Lacoste B, Gu C (2015) Neuronal and vascular interactions. *Annu Rev Neurosci* 38:25–46.
51. Harb R, Whiteus C, Freitas C, Grutzendler J (2013) In vivo imaging of cerebral microvascular plasticity from birth to death. *J Cereb Blood Flow Metab* 33(1):146–156.
52. Lacoste B, et al. (2014) Sensory-related neural activity regulates the structure of vascular networks in the cerebral cortex. *Neuron* 83(5):1117–1130.
53. Whiteus C, Freitas C, Grutzendler J (2014) Perturbed neural activity disrupts cerebral angiogenesis during a postnatal critical period. *Nature* 505(7483):407–411.
54. Blüml S, et al. (2013) Metabolic maturation of the human brain from birth through adolescence: Insights from in vivo magnetic resonance spectroscopy. *Cereb Cortex* 23(12):2944–2955.
55. Blüml S, Wisnowski JL, Nelson MD, Jr, Paquette L, Panigrahy A (2014) Metabolic maturation of white matter is altered in preterm infants. *PLoS One* 9(1):e85829.
56. da Costa CS, Greisen G, Austin T (2015) Is near-infrared spectroscopy clinically useful in the preterm infant? *Arch Dis Child Fetal Neonatal Ed* 100(6):F558–F561.
57. Hoshi Y (2016) Hemodynamic signals in fNIRS. *Prog Brain Res* 225:153–179.
58. Batschelet E (1981) *Circular Statistics in Biology* (Academic, London), Vol 371.